


Cite this: *RSC Adv.*, 2021, 11, 3012

# Understanding the effect of oxide components on proton mobility in phosphate glasses using a statical analysis approach†

Takahisa Omata,<sup>a</sup> Issei Suzuki,<sup>a</sup> Aman Sharma,<sup>a</sup> Tomohiro Ishiyama,<sup>b</sup> Junji Nishii,<sup>c</sup> Toshiharu Yamashita<sup>d</sup> and Hiroshi Kawazoe<sup>d</sup>

The models to describe the proton mobility ( $\mu_H$ ) together with the glass transition temperature ( $T_g$ ) of proton conducting phosphate glasses employing the glass composition as descriptors have been developed using a statical analysis approach. According to the models, the effects of additional  $\text{HO}_{1/2}$ ,  $\text{MgO}$ ,  $\text{BaO}$ ,  $\text{LaO}_{3/2}$ ,  $\text{WO}_3$ ,  $\text{NbO}_{5/2}$ ,  $\text{BO}_{3/2}$  and  $\text{GeO}_2$  as alternative to  $\text{PO}_{5/2}$  were found as following.  $\mu_H$  at  $T_g$  is determined first by concentrations of  $\text{HO}_{1/2}$  and  $\text{PO}_{5/2}$ , and  $\mu_H$  at  $T_g$  increases with increasing  $\text{HO}_{1/2}$  concentration and decreasing  $\text{PO}_{5/2}$ . The component oxides are categorized into three groups according to the effects on  $\mu_H$  at  $T_g$  and  $T_g$ . The group 1 oxides increase  $\mu_H$  at  $T_g$  and decrease  $T_g$ , and  $\text{HO}_{1/2}$ ,  $\text{MgO}$ ,  $\text{BaO}$  and  $\text{LaO}_{3/2}$  and  $\text{BO}_{3/2}$  are involved in this group. The group 2 oxides increase both  $\mu_H$  at  $T_g$  and  $T_g$ , and  $\text{WO}_3$  and  $\text{GeO}_2$  are involved in this group. The group 3 oxides increase  $T_g$  but do not vary  $\mu_H$  at  $T_g$ . Only  $\text{NbO}_{5/2}$  falls into the group 3 among the oxides examined in this study. The origin of the effect of respective oxide groups on  $\mu_H$  at  $T_g$  and  $T_g$  were discussed.

Received 8th December 2020

Accepted 5th January 2021

DOI: 10.1039/d0ra10327f

rsc.li/rsc-advances

## Introduction

Inorganic glasses have been studied for decades as solid electrolytes because of their electrochemical stability and chemical durability, and various cationic conduction, such as  $\text{Li}^+$ ,  $\text{Ag}^+$  and  $\text{H}^+$  conduction, in oxide glass has been investigated extensively.<sup>1–3</sup> Recent demands for highly proton conducting electrolytes in the temperature range between 250 and 500 °C that is operating temperatures of intermediate temperature fuel cells accelerate to explore proton conducting glasses.<sup>4–9</sup> Our group developed a technique termed as alkali-proton substitution (APS) that injects high concentration of proton carriers,  $>10^{21} \text{ cm}^{-3}$ , into phosphate glasses<sup>10</sup> and fabricated many proton conducting glasses by using APS.<sup>11–14</sup> We studied characteristics of glasses that influence on proton conductivity, such as polymerization level of phosphate framework (ratio of the number of oxygen to phosphorous atoms; O/P ratio)<sup>15</sup> and kinds of glass

network modifier,<sup>16</sup> and the effect of additional glass-network formers, such as  $\text{GeO}_2$ , on the thermal stability.<sup>17</sup> As a result,  $2 \times 10^{-3} \text{ S cm}^{-1}$  of proton conductivity at 300 °C has been achieved by  $34\text{HO}_{1/2}-2\text{NaO}_{1/2}-4\text{NbO}_{5/2}-2\text{BaO}-4\text{LaO}_{3/2}-4\text{GeO}_2-1\text{BO}_{3/2}-49\text{PO}_{5/2}$  glass (36H-glass) up to now.<sup>18</sup> Based on the electromotive force and electrochemical hydrogen pump experiments, the phosphate glass electrolyte is confirmed that the mean transport number of proton is unity even under the oxidation atmosphere like an air electrode atmosphere in the fuel cell,<sup>19</sup> suggesting that highly efficient operation of fuel cells and steam electrolysis cells is achievable owing to its no electronic leakage.<sup>20</sup> In addition, fabrication of ultra-thin glass electrolytes with a thickness of 16  $\mu\text{m}$  was recently demonstrated by the press forming.<sup>21</sup> This will be a great advantage of the glass electrolyte in order to reduce electrolyte resistance (ohmic resistance) of the electrochemical cells. However, further increase of their proton conductivity  $>1 \times 10^{-2} \text{ S cm}^{-1}$  at the operating temperature is still required for practical applications.

Very recently, we have found that the mobility of proton carriers ( $\mu_H$ ) at the glass transition temperature ( $T_g$ ) in phosphate glasses converges in a small range between  $2 \times 10^{-9}$  and  $2 \times 10^{-7} \text{ cm}^2 \text{ V}^{-1} \text{ s}^{-1}$ , whereas  $T_g$  of the glasses is in the wide range of 150 to 650 °C, proton conductivity at 200 °C is also wide range of  $10^{-10}$  to  $10^{-4} \text{ S cm}^{-1}$ , and proton carrier concentration is in the range of  $10^{19}$  to  $10^{22} \text{ cm}^{-3}$ .<sup>22</sup> Because the  $\mu_H$  at  $T_g$  of the 36H-glass is  $5.4 \times 10^{-8} \text{ cm}^2 \text{ V}^{-1} \text{ s}^{-1}$  that is the middle in the  $\mu_H$  at  $T_g$  range from  $2 \times 10^{-9}$  to  $2 \times 10^{-7} \text{ cm}^2 \text{ V}^{-1} \text{ s}^{-1}$ , it is suggested that its proton conductivity can be further increased by

<sup>a</sup>Institute of Multidisciplinary Research for Advanced Materials, Tohoku University, Katahira 2-1-1, Sendai 980-8577, Japan. E-mail: takahisa.omata.c2@tohoku.ac.jp; Fax: +81-22-217-5832; Tel: +81-22-217-5832

<sup>b</sup>Fuel Cell Materials Group, Research Institute for Energy Conservation, National Institute of Advanced Industrial Science and Technology (AIST), AIST Central 5, Higashi 1-1-1, Tsukuba, Ibaraki 305-8565, Japan

<sup>c</sup>Research Institute for Electronic Science, Hokkaido University, Kita 21 Nishi 10, Kitaku, Sapporo 001-0021, Japan

<sup>d</sup>Kawazoe Frontier Technologies Corporation, Kuden-cho 931-113, Sakae-ku, Yokohama 247-0014, Japan

† Electronic supplementary information (ESI) available. See DOI: 10.1039/d0ra10327f



improving the  $\mu_{\text{H}}$  at  $T_{\text{g}}$ . Because the determining factor of  $\mu_{\text{H}}$  at  $T_{\text{g}}$  of proton conducting phosphate glasses has yet to be cleared, we unfortunately still do not understand how to improve  $\mu_{\text{H}}$  at  $T_{\text{g}}$ .

The composition of glasses is continually controllable unlike the crystalline materials; therefore, various properties of glasses, have been empirically expressed by the mole fraction weighting mean of the respective components.<sup>23–26</sup> Whereas to understand the effects of fundamental properties of glasses, such as O–H bonding, local structure surrounding protons and short range atomic structure of the glass framework, on  $\mu_{\text{H}}$  at  $T_{\text{g}}$  are of course important to understand the proton conduction in phosphate glasses from the physical aspect, understanding the relationship between the glass composition and  $\mu_{\text{H}}$  at  $T_{\text{g}}$  is also valuable in order to improve the electrolyte performance of proton conducting phosphate glasses. When the proton conductivity is successfully described by the glass composition, the proton conductivity of phosphate glasses will be easy to improve based on the obtained relationship between the glass composition and  $\mu_{\text{H}}$  at  $T_{\text{g}}$ , and that will have a major impact on the electrochemical cells such as fuel cells and steam electrolysis cells working at intermediate temperatures. The proton conducting phosphate glasses prepared by using APS previously reported consists of many oxide components;<sup>22</sup> for example, 36H-glass involves 8 oxides as  $\text{HO}_{1/2}$ ,  $\text{NaO}_{1/2}$ ,  $\text{BaO}$ ,  $\text{LaO}_{3/2}$ ,  $\text{NbO}_{5/2}$ ,  $\text{GeO}_2$ ,  $\text{BO}_{3/2}$  and  $\text{PO}_{5/2}$ ; therefore, it is not easy to understand the role of the respective component oxides on  $\mu_{\text{H}}$  at  $T_{\text{g}}$  and the relationship between the composition and  $\mu_{\text{H}}$  at  $T_{\text{g}}$ .

Here, we have developed a model, using a statical analysis approach, to describe  $\mu_{\text{H}}$  at  $T_{\text{g}}$  of phosphate glasses according to the glass composition, *i.e.*, the mol% of respective component oxides were employed as descriptors. We also developed a model to describe  $T_{\text{g}}$  because the thermal stability of proton conducting glasses is another key property taking the working temperature of the electrochemical devices involving the glasses into account. The effect of respective component oxides on  $\mu_{\text{H}}$  at  $T_{\text{g}}$  and  $T_{\text{g}}$  were discussed based on the model obtained.

## Methodology

### Dataset details

The dataset for  $\mu_{\text{H}}$  at  $T_{\text{g}}$  and  $T_{\text{g}}$  of proton conducting phosphate glasses used as training data in this study is referenced from previous report (Table 1 in ref. 16). The dataset has originally 32 records, but for the 13 records in the original dataset, the proton carrier concentrations are smaller than 1 mol% because the proton carrier in those 13 glasses are originated from the residual water. Therefore, we used a dataset that consists of remaining 19 records as summarized in Table 1. Each record contains glass composition in mol% and experimentally determined  $\mu_{\text{H}}$  at  $T_{\text{g}}$  and  $T_{\text{g}}$ .

### Regression models and method

A linear combination model, in which mol% of respective oxides are used as predictors, is employed for both  $\log(\mu_{\text{H}}$  at  $T_{\text{g}})$

and  $T_{\text{g}}$  in this study. The regression algorithm used in this study is based on the linear regression as implemented in MATLAB (MathWorks, USA). When the general linear regression was preliminary performed for  $\log(\mu_{\text{H}}$  at  $T_{\text{g}})$ , the overtraining occurred maybe because of small number of training data; the predicted  $\mu_{\text{H}}$  at  $T_{\text{g}}$  for the 55 296 glass compositions described later was unreasonable values in the range of  $10^{-29}$  to  $10^{17} \text{ cm}^2 \text{ V}^{-1} \text{ s}^{-1}$  (Fig. S1 and S2 in ESI†), although the range of the experimentally observed values is in the range of  $2 \times 10^{-9}$  to  $2 \times 10^{-7} \text{ cm}^2 \text{ V}^{-1} \text{ s}^{-1}$ .<sup>22</sup> Therefore, we employed the principal components analysis to fit a linear regression in order to avoid overtraining. Five principal components were employed to explain 95% of variance of original data. The mathematical model can be written as

$$\log(\mu_{\text{H}} \text{ at } T_{\text{g}} / \text{cm}^2 \text{ V}^{-1} \text{ s}^{-1}) = a_0 + \sum_{n=1}^5 a_n \text{PC}_n \quad (1)$$

$$T_{\text{g}} / ^\circ\text{C} = b_0 + \sum_{n=1}^5 b_n \text{PC}'_n \quad (2)$$

$$\text{PC}_n = \sum_i c_i x_i \quad (3)$$

where  $\text{PC}_n$  and  $\text{PC}'_n$  are  $n$ th principal component explaining the variance of experimentally observed  $\log(\mu_{\text{H}}$  at  $T_{\text{g}})$  and  $T_{\text{g}}$ , respectively,  $a_0$  and  $b_0$  are intercepts,  $a_n$  and  $b_n$  are coefficients of  $n$ th principal component,  $x_i$  is the mol% of the oxide  $i$ , and  $c_i$  is its coefficient.

In order to check the validity of the models and to understand the effect of respective component oxides on  $\mu_{\text{H}}$  at  $T_{\text{g}}$  and  $T_{\text{g}}$ , we performed to predict  $\mu_{\text{H}}$  at  $T_{\text{g}}$  and  $T_{\text{g}}$  for 55 296 glass compositions containing 30, 33 and 36 mol% of  $\text{HO}_{1/2}$ , 0, 2 and 4 mol% of  $\text{WO}_3$ , 0, 2, 4 and 6 mol% of  $\text{NbO}_{5/2}$ , 0, 2, 4 and 6 mol% of  $\text{MgO}$ , 0, 2, 4 and 6 mol% of  $\text{BaO}$ , 0, 2, 4 and 6 mol% of  $\text{LaO}_{3/2}$ , 0, 1, 2, 3, 4 and 5 mol% of  $\text{GeO}_2$ , 0, 1, 2 and 3 mol% of  $\text{BO}_{3/2}$  and 28–70 mol% of  $\text{PO}_{5/2}$ . In this prediction, all the compositions were assumed to form homogeneous glasses.

## Results and discussion

### Linear regression models for $\mu_{\text{H}}$ at $T_{\text{g}}$ and $T_{\text{g}}$

The following relationships of  $\log(\mu_{\text{H}}$  at  $T_{\text{g}})$  and  $T_{\text{g}}$  against the five principal components of glass composition were obtained after regression:

$$\log(\mu_{\text{H}} \text{ at } T_{\text{g}}) = -7.8549 + 0.022233 \times \text{PC}_1 - 0.01167 \times \text{PC}_2 + 0.26874 \times \text{PC}_3 - 0.01727 \times \text{PC}_4 + 0.160456 \times \text{PC}_5, \quad (4)$$

$$T_{\text{g}} = 204.368 - 1.622 \times \text{PC}'_1 + 1.282 \times \text{PC}'_2 - 2.350 \times \text{PC}'_3 + 7.897 \times \text{PC}'_4 + 5.630 \times \text{PC}'_5, \quad (5)$$

The principal components are summarized in Tables 2 and 3 for  $\log(\mu_{\text{H}}$  at  $T_{\text{g}})$  and  $T_{\text{g}}$ , respectively. Fig. 1(a) and (b) show comparison of experimentally observed and predicted values of  $\mu_{\text{H}}$  at  $T_{\text{g}}$  and  $T_{\text{g}}$ , respectively, for the 19 training data. The root mean square error (RMSE) was 0.2775 for  $\log(\mu_{\text{H}}$  at  $T_{\text{g}})$  and was



**Table 1** Training dataset of the relationship between the glass compositions and the proton mobility ( $\mu_H$ ) at the glass transition temperature ( $T_g$ ) and  $T_g$ 

Mol% of component oxide																
No.	HO <sub>1/2</sub>	NaO <sub>1/2</sub>	WO <sub>3</sub>	NbO <sub>5/2</sub>	TaO <sub>5/2</sub>	MgO	BaO	LaO <sub>3/2</sub>	AlO <sub>3/2</sub>	YO <sub>3/2</sub>	GdO <sub>3/2</sub>	GeO <sub>2</sub>	BO <sub>3/2</sub>	PO <sub>5/2</sub>	$\mu_{\text{H}}$ at $T_{\text{g}}$ (cm <sup>2</sup> V <sup>-1</sup> s <sup>-1</sup> )	$T_{\text{g}}$ (°C)
1	25	3	1	8	0	0	0	5	0	0	0	0	0	58	$2.1 \times 10^{-9}$	200
2	24	8	1	8	0	0	0	5	0	0	0	0	0	54	$5.5 \times 10^{-9}$	177
3	25	10	1	8	0	0	0	5	0	0	0	0	0	51	$3.7 \times 10^{-8}$	190
4	32	6	1	8	0	0	0	5	0	0	0	0	0	48	$3.7 \times 10^{-8}$	170
5	32	8	1	8	0	0	0	5	0	0	0	0	0	46	$1.2 \times 10^{-8}$	167
6	28	2	1	8	0	0	0	5	3	3	0	0	0	50	$2.0 \times 10^{-8}$	281
7	29	6	1	8	0	0	0	5	3	0	0	0	0	48	$7.6 \times 10^{-9}$	224
8	30	5	1	8	0	0	0	5	0	3	0	0	0	48	$4.1 \times 10^{-9}$	228
9	35	0	0	3	0	5	0	3	0	0	0	2	2	50	$1.3 \times 10^{-8}$	192
10	32	3	0	3	0	0	5	3	0	0	0	2	2	50	$6.8 \times 10^{-9}$	163
11	34	2	0	4	0	0	2	4	0	0	0	4	1	49	$5.4 \times 10^{-8}$	180
12	38	2	0	0	4	2	0	4	0	0	0	2	1	47	$2.7 \times 10^{-8}$	165
13	17	8	0	0	0	0	0	8	0	0	0	1	0	66	$2.6 \times 10^{-9}$	227
14	12	13	0	0	0	0	0	6	0	0	0	6	0	63	$1.3 \times 10^{-8}$	243
15	33	2	0	0	0	2	0	5	0	0	0	5	0	53	$4.0 \times 10^{-8}$	182
16	31	4	0	0	0	2	0	0	0	0	5	5	0	53	$1.2 \times 10^{-8}$	178
17	20	5	0	0	0	0	0	6	0	0	0	6	0	63	$1.5 \times 10^{-8}$	252
18	28	7	0	0	0	2	0	0	0	0	5	5	0	53	$1.4 \times 10^{-8}$	233
19	34	1	8	8	0	0	0	5	0	0	0	0	0	44	$1.1 \times 10^{-7}$	231

**Table 2** Five principal components obtained from the analysis of  $\mu_H$  at  $T_g$ 

Principal components	PC <sub>1</sub>	PC <sub>2</sub>	PC <sub>3</sub>	PC <sub>4</sub>	PC <sub>5</sub>
Proportion of variance	0.659	0.183	0.061	0.026	0.021
Cumulative proportion	0.659	0.842	0.903	0.929	0.950
Factor loading					
$x(\text{HO}_{1/2})$	0.69239	-0.32693	-0.07750	-0.19571	-0.15439
$x(\text{NaO}_{1/2})$	-0.24549	0.28854	0.71623	-0.35865	-0.03489
$x(\text{WO}_3)$	0.06837	0.15986	-0.11444	0.32222	0.77387
$x(\text{NbO}_{5/2})$	0.16670	0.68417	-0.16598	0.28247	-0.30664
$x(\text{TaO}_{5/2})$	0.02694	-0.05991	0.00355	-0.24336	0.04874
$x(\text{MgO})$	0.03954	-0.18457	0.01768	0.06160	-0.13778
$x(\text{BaO})$	0.02319	-0.04547	-0.02005	-0.12335	-0.09325
$x(\text{LaO}_{3/2})$	-0.08309	0.19943	-0.33952	-0.50726	0.26128
$x(\text{AlO}_{3/2})$	0.01281	0.06277	-0.04134	0.08739	-0.09090
$x(\text{YO}_{3/2})$	0.01467	0.05828	-0.05950	0.09692	-0.09979
$x(\text{GdO}_{3/2})$	-0.00319	-0.15212	0.31784	0.52266	-0.11954
$x(\text{GeO}_2)$	-0.10164	-0.37370	0.21746	0.08717	0.28694
$x(\text{BO}_{3/2})$	0.02654	-0.05917	-0.04343	-0.10435	-0.08555
$x(\text{PO}_{5/2})$	-0.63774	-0.25119	-0.41100	0.07224	-0.24811

23.6 °C for  $T_g$ . No systematic error was observed and the fitting were reasonably good for both  $\log(\mu_H \text{ at } T_g)$  and  $T_g$ . Fig. 2(a) and (b) respectively show the predicted values of  $\log(\mu_H \text{ at } T_g)$  and  $T_g$  for the 55 296 phosphate glass compositions. The predicted values are ranging between  $8.1 \times 10^{-10}$  and  $7.7 \times 10^{-7} \text{ cm}^2 \text{V}^{-1} \text{s}^{-1}$  for  $\mu_H$  at  $T_g$  and between 152 and 256 °C for  $T_g$ . As compared with experimentally determined  $\mu_H$  at  $T_g$ ,<sup>22</sup> the range of the predicted values are very close to the range of the experimentally observed values from  $2 \times 10^{-9}$  to  $2 \times 10^{-7} \text{ cm}^2 \text{V}^{-1} \text{s}^{-1}$ . These results indicate that the models obtained are quite reasonable and available to discuss the effects of respective component oxides on  $\mu_H$  at  $T_g$ .

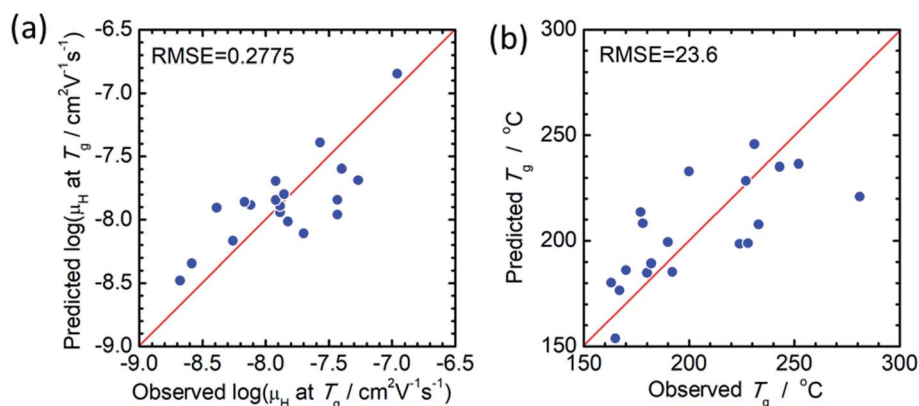
As seen in Table 2, absolute values of the factor loading of HO<sub>1/2</sub> and PO<sub>5/2</sub> components are particularly larger than those

of the other components, indicating that  $\mu_H$  at  $T_g$  is first determined by the concentration of HO<sub>1/2</sub> and PO<sub>5/2</sub>. Taking into account that the coefficient of PC<sub>1</sub> in eqn (4) is positive,  $\mu_H$  at  $T_g$  increases with the increasing HO<sub>1/2</sub> concentration, and it reduces with the increasing PO<sub>5/2</sub> concentration. In this respect, the experimental observation that the  $\mu_H$  increases with the decreasing polymerization level of phosphate glass-network is reproduced well by the present model.  $\mu_H$  turns into decrease at O/P ratio (ratio of the number of oxygen to phosphorous atoms) higher than 3.5–3.6;<sup>15</sup> however, such a behavior cannot be reproduced using linear regression model. Consequently, applicable composition range of the present model is limited in a O/P ratio smaller than 3.5–3.6.



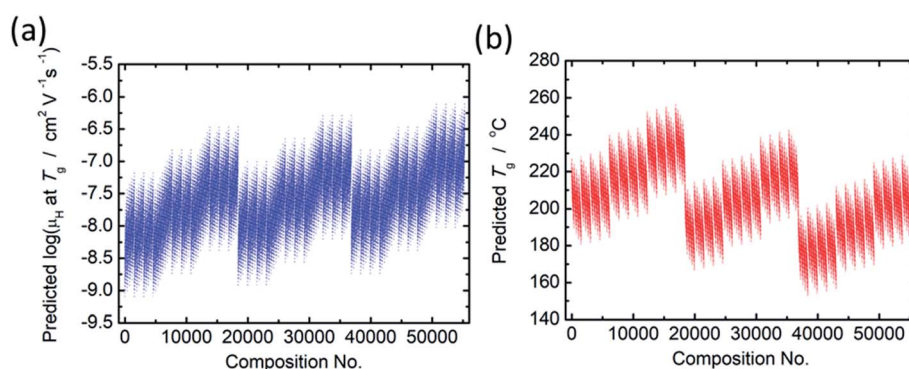
Table 3 Five principal components obtained from the analysis of  $T_g$ 

Principal components	PC <sub>1</sub>	PC <sub>2</sub>	PC <sub>3</sub>	PC <sub>4</sub>	PC <sub>5</sub>
Proportion of variance	0.659	0.183	0.061	0.026	0.021
Cumulative proportion	0.659	0.842	0.903	0.929	0.950
Factor loading					
$x(\text{HO}_{1/2})$	0.69239	-0.32693	-0.0775	-0.19571	-0.15439
$x(\text{NaO}_{1/2})$	-0.24549	0.28854	0.71623	-0.35865	-0.03489
$x(\text{WO}_3)$	0.06837	0.15986	-0.11444	0.32222	0.77387
$x(\text{NbO}_{5/2})$	0.1667	0.68417	-0.16598	0.28247	-0.30664
$x(\text{TaO}_{5/2})$	0.02694	-0.05991	0.00355	-0.24336	0.04874
$x(\text{MgO})$	0.03954	-0.18457	0.01768	0.0616	-0.13778
$x(\text{BaO})$	0.02319	-0.04547	-0.02005	-0.12335	-0.09325
$x(\text{LaO}_{3/2})$	-0.08309	0.19943	-0.33952	-0.50726	0.26128
$x(\text{AlO}_{3/2})$	0.01281	0.06277	-0.04134	0.08739	-0.0909
$x(\text{YO}_{3/2})$	0.01467	0.05828	-0.0595	0.09692	-0.09979
$x(\text{GdO}_{3/2})$	-0.00319	-0.15212	0.31784	0.52266	-0.11954
$x(\text{GeO}_2)$	-0.10164	-0.3737	0.21746	0.08717	0.28694
$x(\text{BO}_{3/2})$	0.02654	-0.05917	-0.04343	-0.10435	-0.08555
$x(\text{PO}_{5/2})$	-0.63774	-0.25119	-0.411	0.07224	-0.24811

Fig. 1 Comparison of experimentally observed and predicted values of (a)  $\mu_{\text{H}}$  at  $T_g$  and (b)  $T_g$ .

From comparison of the models of  $\mu_{\text{H}}$  at  $T_g$  and  $T_g$  as summarized in Tables 2 and 3, the factor loadings of respective principal components for  $\log(\mu_{\text{H}}$  at  $T_g$ ) and  $T_g$  are surprisingly found to be the same each other, *i.e.*, the variance in both  $\log(\mu_{\text{H}}$  at  $T_g$ ) and  $T_g$  are explained by the same principal components, clearly indicating that there should be some kind of relationship between  $\log(\mu_{\text{H}}$  at  $T_g$ ) and  $T_g$ . This is quite consistent with

our previously reported estimation that the motion of protons (proton diffusion or mobility) determines the motion of glass framework ( $T_g$ ) in the proton conducting phosphate glasses.<sup>22</sup> Fig. 3 shows  $\log(\mu_{\text{H}}$  at  $T_g$ ) as a function of  $T_g$  of 55 296 predicted values (black dots) together with the experimentally observed 19 values (red dots). A trend that  $\log(\mu_{\text{H}}$  at  $T_g$ ) decreases linearly with the increasing  $T_g$  was clearly observed for the predicted

Fig. 2 Predicted values of (a)  $\log(\mu_{\text{H}}$  at  $T_g$ ) and (b)  $T_g$  for the 55 296 phosphate glass compositions.



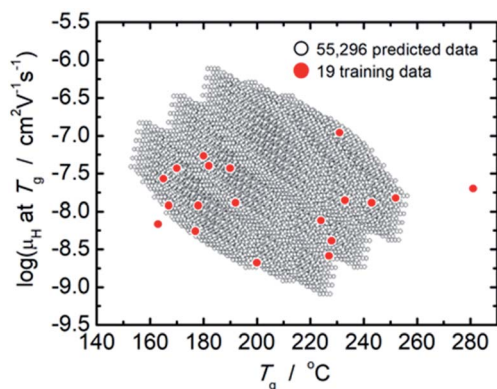


Fig. 3 Plot of  $\log(\mu_{\text{H}} \text{ at } T_{\text{g}})$  as a function of  $T_{\text{g}}$  of 55 296 predicted values (open black dots) together with the experimentally observed 19 values (closed red dots).

values in Fig. 3. The observed relationship between  $\log(\mu_{\text{H}} \text{ at } T_{\text{g}})$  and  $T_{\text{g}}$  may be a key to understand physical factor to determine  $\mu_{\text{H}} \text{ at } T_{\text{g}}$ ; however, we need additional information in order to go further this problem. Therefore, the origin of the relationship between  $\log(\mu_{\text{H}} \text{ at } T_{\text{g}})$  and  $T_{\text{g}}$  remains as an open question, and we do not discuss further in this paper.

#### Effects of respective component oxides on $\mu_{\text{H}}$ at $T_{\text{g}}$ and $T_{\text{g}}$

As mentioned in the previous section, there is a clear relationship between  $\log(\mu_{\text{H}} \text{ at } T_{\text{g}})$  and  $T_{\text{g}}$ ; therefore, the effect of each component oxide was studied in this regard. Fig. 4 shows the distribution of relationship between  $\log(\mu_{\text{H}} \text{ at } T_{\text{g}})$  and  $T_{\text{g}}$  depending on the concentration of respective component oxides. All data plotted in Fig. 4 are predicted values. In Fig. 4(a), 55 296 predicted values are distinguished into three parts depending on the concentration of  $\text{HO}_{1/2}$ . In Fig. 4(b), 18 432 predicted values for the glasses with 30 mol% of  $\text{HO}_{1/2}$  are plotted and they are distinguished into three parts depending on the concentration of  $\text{WO}_3$ . In Fig. 4(c), 6144 predicted values for the glasses with 30 mol% of  $\text{HO}_{1/2}$  and 0 mol% of  $\text{WO}_3$  are plotted and they are distinguished into four parts depending on the concentration of  $\text{LaO}_{3/2}$ . In Fig. 4(d), (e), (f), (g) and (h), 1536 predicted values for the glasses with 30 mol% of  $\text{HO}_{1/2}$ , 0 mol% of  $\text{WO}_3$  and 0 mol% of  $\text{LaO}_{3/2}$  are plotted and they are distinguished into four or six parts depending on the concentration of the oxide of interest ( $\text{MgO}$ ,  $\text{BaO}$ ,  $\text{NbO}_{5/2}$ ,  $\text{BO}_{3/2}$  and  $\text{GeO}_2$ ). The situation observed, when the component oxide of interest adds into the glass as alternative to  $\text{PO}_{5/2}$ , is described as follows.

With the increasing  $\text{HO}_{1/2}$  concentration (Fig. 4(a)), the  $T_{\text{g}}$  decreases by  $5^\circ\text{C}$  per 1 mol%  $\text{HO}_{1/2}$  and  $\log(\mu_{\text{H}} \text{ at } T_{\text{g}})$  increases by 0.06 per 1 mol% of  $\text{HO}_{1/2}$ . In contrast to the dependence of  $\text{HO}_{1/2}$  concentration, both  $T_{\text{g}}$  and  $\log(\mu_{\text{H}} \text{ at } T_{\text{g}})$  increases with the increasing  $\text{WO}_3$  concentration by  $6.5^\circ\text{C}$  and 0.08 per 1 mol% of  $\text{WO}_3$ , respectively (Fig. 4(b)). In the case of  $\text{LaO}_{3/2}$  shown in Fig. 4(c),  $T_{\text{g}}$  decreases with the increasing  $\text{LaO}_{3/2}$  concentration by  $2.2^\circ\text{C}$  per 1 mol% of  $\text{LaO}_{3/2}$ , and  $\log(\mu_{\text{H}} \text{ at } T_{\text{g}})$  increases with the increasing  $\text{LaO}_{3/2}$  concentration by 0.1 per 1 mol% of  $\text{LaO}_{3/2}$ . In the cases for  $\text{MgO}$ ,  $\text{BaO}$  and  $\text{BO}_{3/2}$  shown in Fig. 4(d), (e) and (f), respectively, the dependence are similar to

the case of  $\text{HO}_{1/2}$  and  $\text{LaO}_{3/2}$ ;  $T_{\text{g}}$  decreases and  $\log(\mu_{\text{H}} \text{ at } T_{\text{g}})$  increases with the increasing concentration of the additional oxide. The variation in  $T_{\text{g}}$  and  $\log(\mu_{\text{H}} \text{ at } T_{\text{g}})$  are respectively  $-1.5^\circ\text{C}$  and 0.05 per 1 mol% of  $\text{MgO}$ ,  $-2.4^\circ\text{C}$  and 0.05 per 1 mol% of  $\text{BaO}$  and  $-2.2^\circ\text{C}$  and 0.05 per 1 mol% of  $\text{BO}_{3/2}$ . For  $\text{NbO}_{5/2}$ , as clearly seen in Fig. 4(g), the relationship between  $\log(\mu_{\text{H}} \text{ at } T_{\text{g}})$  and  $T_{\text{g}}$  is little dependent on the  $\text{NbO}_{5/2}$  concentration, i.e.,  $T_{\text{g}}$  increases by  $0.7^\circ\text{C}$  per 1 mol% of  $\text{NbO}_{5/2}$  and  $\log(\mu_{\text{H}} \text{ at } T_{\text{g}})$  does not change regardless  $\text{NbO}_{5/2}$  concentration. In the case of  $\text{GeO}_2$  shown in Fig. 4(h), both  $T_{\text{g}}$  and  $\log(\mu_{\text{H}} \text{ at } T_{\text{g}})$  increases with the increasing  $\text{GeO}_2$  concentration similar to the case of  $\text{WO}_3$ ; however, increase in  $T_{\text{g}}$ ,  $0.6^\circ\text{C}$  per 1 mol% of  $\text{GeO}_2$ , is much smaller than that of  $\text{WO}_3$  ( $6.5^\circ\text{C}$  per 1 mol% of  $\text{WO}_3$ ), while increase in  $\log(\mu_{\text{H}} \text{ at } T_{\text{g}})$ , 0.12 per 1 mol% of  $\text{GeO}_2$ , is slightly larger than that of  $\text{WO}_3$  (0.08 per 1 mol% of  $\text{WO}_3$ ). These situations are summarized in Table 4.

It is noticed that the component oxides are categorized into three groups in terms of the effect on the  $\mu_{\text{H}}$  at  $T_{\text{g}}$  and  $T_{\text{g}}$ . The group 1 consists of  $\text{HO}_{1/2}$ ,  $\text{MgO}$ ,  $\text{BaO}$ ,  $\text{LaO}_{3/2}$  and  $\text{BO}_{3/2}$ . They increase  $\mu_{\text{H}}$  at  $T_{\text{g}}$  but decrease  $T_{\text{g}}$ , when their concentrations increase. The group 2 involves  $\text{WO}_3$  and  $\text{GeO}_2$  that increase both  $\mu_{\text{H}}$  at  $T_{\text{g}}$  and  $T_{\text{g}}$ , when their concentrations increase. The group 3 consists of  $\text{NbO}_{5/2}$  only in the present study, and it increases  $T_{\text{g}}$  but does not changes  $\mu_{\text{H}}$  at  $T_{\text{g}}$ , when its concentration increases. Such effects categorized into three groups could not be found in the experimentally observed data, i.e., 19 glass compositions that used as training data in this study. The information of the three groups is useful to obtain purpose-designed glasses.

The effect on  $T_{\text{g}}$  of respective group oxides is quite reasonable and explained according to the glass structural chemistry as following. The group 1 consists of the glass-modifiers except for  $\text{BO}_{3/2}$ ; therefore, the reduction of  $T_{\text{g}}$  with the increasing concentration of the group 1 oxide is reasonably understood as a result of breaking of the phosphate glass-network by introduction of the glass-modifier oxides.  $\text{BO}_{3/2}$  is a glass-former oxide, and it may exist in the glass as the trigonal planar  $\text{BO}_3$  in addition to the  $\text{BO}_4$  tetrahedron in the phosphate glasses assumed in the present study.<sup>27–29</sup> When the trigonal planar  $\text{BO}_3$  is introduced into the glass as alternative to  $\text{PO}_4$  tetrahedra, the number of the bridging oxygens in the glass-network reduces as the concentration of the trigonal planar  $\text{BO}_3$  increases. Consequently,  $\text{BO}_{3/2}$  acts as almost glass-modifier, and its effect on  $T_{\text{g}}$  is similar to the other group 1 oxides that are glass-modifier oxides. The groups 2 and 3 consist of the oxides exhibiting high glass forming ability, i.e.,  $\text{GeO}_2$  is a glass-former and  $\text{WO}_3$  and  $\text{NbO}_{5/2}$  are conditional glass-formers.<sup>30</sup> When the groups 2 and 3 oxides are introduced into the glass as alternative to  $\text{PO}_{5/2}$ ,  $\text{GeO}_2$  tetrahedra and  $\text{WO}_6$  and  $\text{NbO}_6$  octahedra strengthen the phosphate glass-network, resulting in increasing  $T_{\text{g}}$ .

In contrast to the effect on  $T_{\text{g}}$ , the origin of the effect on  $\mu_{\text{H}}$  at  $T_{\text{g}}$  is still an open question as already mentioned. However, the effect of the group 2 oxides, i.e., they increase  $\mu_{\text{H}}$  at  $T_{\text{g}}$  with the increasing their concentration, may be explained phenomenologically as following. For the effect of  $\text{WO}_3$ , we refer to the heteropoly acid of  $\text{WO}_3$  combined with  $\text{PO}_{5/2}$ . It is well known



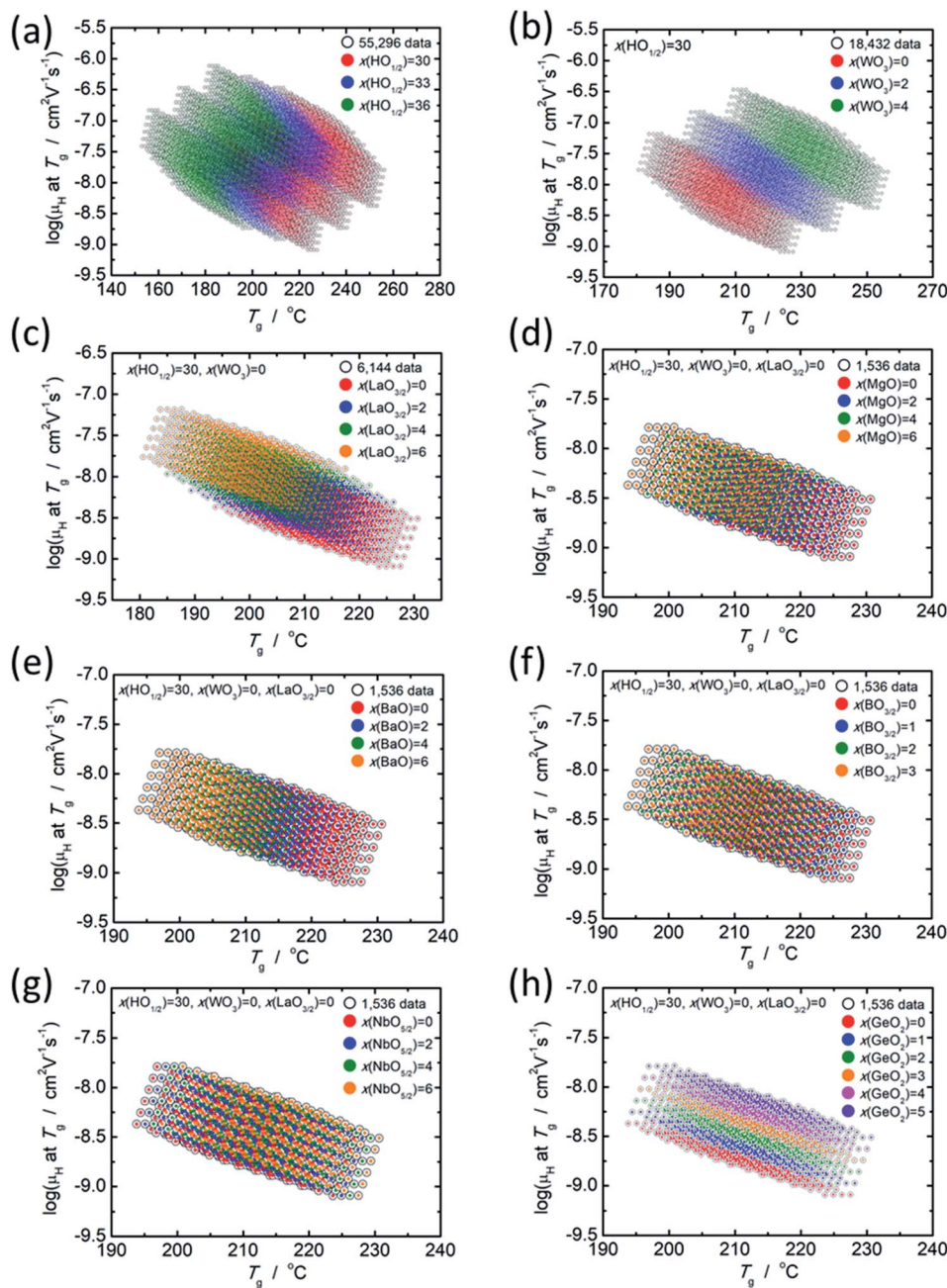


Fig. 4 Distribution of the relationship between predicted values of  $\log(\mu_{\text{H}} \text{ at } T_{\text{g}})$  and  $T_{\text{g}}$  depending on the concentration of respective component oxides. (a) 55 296 predicted values distinguished by the  $\text{HO}_{1/2}$  concentration (red dots = 30 mol%  $\text{HO}_{1/2}$ , blue dots = 33 mol%  $\text{HO}_{1/2}$  and green dots = 36 mol%  $\text{HO}_{1/2}$ ). (b) 18 432 predicted values for the glasses with 30 mol% of  $\text{HO}_{1/2}$  distinguished by the  $\text{WO}_3$  concentration (red dots = 0 mol%  $\text{WO}_3$ , blue dots = 2 mol%  $\text{WO}_3$  and green dots = 4 mol%  $\text{WO}_3$ ). (c) 6144 predicted values for the glasses with 30 mol% of  $\text{HO}_{1/2}$  and 0 mol% of  $\text{WO}_3$  distinguished by the  $\text{LaO}_{3/2}$  concentration (red dots = 0 mol%  $\text{LaO}_{3/2}$ , blue dots = 2 mol%  $\text{LaO}_{3/2}$ , green dots = 4 mol%  $\text{LaO}_{3/2}$  and orange dots = 6 mol%  $\text{LaO}_{3/2}$ ). (d), (e), (f), (g) and (h) 1536 predicted values for the glasses with 30 mol% of  $\text{HO}_{1/2}$ , 0 mol% of  $\text{WO}_3$  and 0 mol% of  $\text{LaO}_{3/2}$  respectively distinguished by the concentration of  $\text{MgO}$ ,  $\text{BaO}$ ,  $\text{BO}_{3/2}$ ,  $\text{NbO}_{5/2}$  and  $\text{GeO}_2$ .

Table 4 Variation of  $\log(\mu_{\text{H}} \text{ at } T_{\text{g}})$  and  $T_{\text{g}}$  with the increasing component oxide by 1 mol%

Component oxide		Group 1				Group 2		Group 3
		MgO	BaO	$\text{LaO}_{3/2}$	$\text{BO}_{3/2}$	$\text{WO}_3$	$\text{GeO}_2$	$\text{NbO}_{5/2}$
Variation per 1 mol% of oxide	$\log(\mu_{\text{H}} \text{ at } T_{\text{g}})$	0.05	0.05	0.10	0.05	0.08	0.12	0.00
	$T_{\text{g}} / ^\circ\text{C}$	−1.5	−2.4	−2.2	−2.2	6.5	0.6	0.7



that  $\text{WO}_3$  and  $\text{PO}_{5/2}$  form heteropoly acid,  $\text{H}_3\text{PW}_{12}\text{O}_{40} \cdot 6\text{H}_2\text{O}$ , and it exhibits strong acidity much stronger than  $\text{H}_2\text{SO}_4$ .<sup>31,32</sup> The strong acidity, *i.e.*, easy proton formation, is explained by dispersion of the negative charge over many atoms of the polyanion,  $\text{PW}_{12}\text{O}_{40}^{3-}$ , and the polarization of the outer  $\text{W}=\text{O}$  bond.<sup>32</sup> Of course, the molar ratio of  $\text{WO}_3$  over against  $\text{PO}_{5/2}$  is much smaller (4 mol% of  $\text{WO}_3$  is the highest, while 28 mol% of  $\text{PO}_{5/2}$  is the lowest) than that of  $\text{PW}_{12}\text{O}_{40}^{3-}$ ; therefore, formation of  $\text{PW}_{12}\text{O}_{40}^{3-}$ -like polyanion should be excluded. However, the  $\text{WO}_3$  coexisting with  $\text{PO}_{5/2}$  may have an effect to enhance acidity of  $\equiv\text{P}-\text{O}-\text{H}$  units. In this case, protons are easy to dissociate from  $\equiv\text{P}-\text{O}-\text{H}$  units; as a result,  $\mu_{\text{H}}$  would be increased by the addition of  $\text{WO}_3$  into phosphate glasses.

In the case of  $\text{GeO}_2$ , we refer to the silicophosphate gel that is prepared by reacting  $\text{SiCl}_4$  with anhydrous phosphoric acid ( $\text{H}_3\text{PO}_4$ ).<sup>33</sup> The silicophosphate gel that involves  $\text{Si}-\text{O}-\text{P}$  bondings exhibits evidently higher proton conductivity than  $\text{H}_3\text{PO}_4$ ,<sup>33,34</sup> although the increase in conductivity is not so large. Taking into account that the polymerization occurs in silicophosphate gel, the concentration of proton carriers in silicophosphate is smaller than that in phosphoric acid, indicating that the  $\text{SiO}_2$  addition enhances  $\mu_{\text{H}}$ . Although the reason why  $\text{SiO}_2$  addition enhance proton conductivity has not been fully understood yet, the octahedrally coordinated  $\text{SiO}_6$  that appears in silicophosphate gel is pointed out as a key feature to explain the effect of  $\text{SiO}_2$  addition into phosphoric acid.<sup>33</sup> While  $\text{GeO}_2$  exhibits similar feature to  $\text{SiO}_2$ , *i.e.*, both  $\text{GeO}_2$  and  $\text{SiO}_2$  are group 4 oxides and exhibit as glass-formers, preference of six-fold coordination of  $\text{Ge}^{4+}$  ion is higher than  $\text{Si}^{4+}$  ion. These imply that  $\text{GeO}_2$  would enhance  $\mu_{\text{H}}$ , when it is added into the phosphoric acid. In this case, increase in  $\mu_{\text{H}}$  by the addition of  $\text{GeO}_2$  to phosphate glass would be understood by the analogous to silicophosphate gel.

## Conclusion

In summary, we developed a linear regression models for the compositional dependence of  $\log(\mu_{\text{H}} \text{ at } T_{\text{g}})$  and  $T_{\text{g}}$  for the proton conducting phosphate glass based on the approach of principal component analysis, and  $\mu_{\text{H}}$  at  $T_{\text{g}}$  and  $T_{\text{g}}$  were predicted for 55 296 of phosphate glasses involving 9 component oxide of  $\text{HO}_{1/2}$ ,  $\text{MgO}$ ,  $\text{BaO}$ ,  $\text{LaO}_{3/2}$ ,  $\text{WO}_3$ ,  $\text{NbO}_{5/2}$ ,  $\text{BO}_{3/2}$ ,  $\text{GeO}_2$  and  $\text{PO}_{5/2}$ . The models themselves do not have any physical meaning of course, but they provide the following information about the effects of respective component oxides on  $\mu_{\text{H}}$  at  $T_{\text{g}}$  and  $T_{\text{g}}$ : (i) the  $\mu_{\text{H}}$  at  $T_{\text{g}}$  is determined first by concentrations of  $\text{HO}_{1/2}$  and  $\text{PO}_{5/2}$ ;  $\mu_{\text{H}}$  at  $T_{\text{g}}$  increases with increasing  $\text{HO}_{1/2}$  concentration and decreasing  $\text{PO}_{5/2}$ . (ii) There is a trend for  $\log(\mu_{\text{H}} \text{ at } T_{\text{g}})$  to increase linearly as  $T_{\text{g}}$  decreases. This is quite consistent with our estimation previously reported that the motion of protons determines the motion of glass framework in the proton conducting phosphate glasses. (iii) The component oxides are categorized into three groups according to the effects on  $\mu_{\text{H}}$  at  $T_{\text{g}}$  and  $T_{\text{g}}$ . The group 1 oxides that behave as glass-modifiers increase  $\mu_{\text{H}}$  at  $T_{\text{g}}$  and decrease  $T_{\text{g}}$ , and  $\text{HO}_{1/2}$ ,  $\text{MgO}$ ,  $\text{BaO}$  and  $\text{LaO}_{3/2}$  and  $\text{BO}_{3/2}$  are involved in this group. The group 2 oxides increase both  $\mu_{\text{H}}$  at  $T_{\text{g}}$  and  $T_{\text{g}}$ , and  $\text{WO}_3$  and  $\text{GeO}_2$  are involved

in this group. The group 3 oxides increase  $T_{\text{g}}$  but do not vary  $\mu_{\text{H}}$  at  $T_{\text{g}}$ . Only  $\text{NbO}_{5/2}$  falls into the group 3 among the oxides examined in this study. These information are very useful to obtain purpose-designed glasses; therefore, they will be applied to the future development of proton-conducting phosphate glasses. Especially, the effects of the additional glass-formers, such as  $\text{GeO}_2$  and  $\text{WO}_3$ , are very important to design highly proton conducting phosphate glass at intermediate temperatures.

The enhance of  $\mu_{\text{H}}$  at  $T_{\text{g}}$  by  $\text{WO}_3$  and  $\text{GeO}_2$  of group 2 oxide is phenomenologically understood by referring to the strong acidity of  $\text{PW}_{12}\text{O}_{40}^{3-}$  heteropoly acid and the enhancing  $\mu_{\text{H}}$  of phosphoric acid by  $\text{SiO}_2$  addition, respectively. In contrast, the origin of the effect of groups 1 and 3 oxides on  $\mu_{\text{H}}$  at  $T_{\text{g}}$  and the relationship between  $\log(\mu_{\text{H}} \text{ at } T_{\text{g}})$  and  $T_{\text{g}}$  still remain as open questions.

## Author contributions

Takahisa Omata: conceptualization, methodology, formal analysis, software, writing – original draft and visualization, Issei Suzuki: validation, visualization and writing – review & editing, Aman Sharma: formal analysis and data curation, Tomohiro Ishiyama: writing – review & editing, Junji Nishii: conceptualization, funding acquisition and writing – review & editing, Toshiharu Yamashita: supervision and writing – review & editing, Hiroshi Kawazoe: supervision and writing – review & editing.

## Conflicts of interest

The authors declare no competing interests.

## Acknowledgements

We thank Prof. Junichi Kawamura (Tohoku University) for valuable comments. This work was supported in part by a Grant-in-Aid for Scientific Research (B) (Grant No. 20H02428). This work was partly performed under the Cooperative Research Program of the “Network Joint Research Center for Materials and Devices” (No. 20194020 and 20204012) and “Dynamic Alliance for Open Innovation Bridging Human, Environment, and Materials”.

## References

- 1 A. Hayashi, A. Sakuda and M. Tatsumisago, *Front. Energy Res.*, 2016, **4**, 1–13.
- 2 M. Nakayama, M. Hanaya, A. Hatate and M. Oguni, *J. Non-Cryst. Solids*, 1994, **172–174**, 1252–1261.
- 3 Y. Abe, H. Hosono, O. Akita and L. L. Hench, *J. Electrochem. Soc.*, 1994, **141**, L64–L65.
- 4 Y. Daiko, *J. Ceram. Soc. Jpn.*, 2013, **121**, 539–543.
- 5 Y. Takamatsu, Y. Daiko, S. Kohara, K. Suzuya, A. Mineshige and T. Yazawa, *Solid State Ionics*, 2013, **245–246**, 19–23.
- 6 H. Sumi, Y. Nakano, Y. Fujishiro and T. Kasuga, *Solid State Sci.*, 2015, **45**, 5–8.



- 7 Y. Huang, E. Christensen, Q. Shuai and Q. Li, *Int. J. Hydrogen Energy*, 2017, **42**, 7235–7240.
- 8 H. Sumi, *J. Ceram. Soc. Jpn.*, 2017, **125**, 829–832.
- 9 S. H. Lee, S. B. Park and Y. Il Park, *Solid State Ionics*, 2020, **345**, 115186.
- 10 T. Ishiyama, S. Suzuki, J. Nishii, T. Yamashita, H. Kawazoe and T. Omata, *J. Electrochem. Soc.*, 2013, **160**, E143–E147.
- 11 T. Ishiyama, S. Suzuki, J. Nishii, T. Yamashita, H. Kawazoe and T. Omata, *Solid State Ionics*, 2014, **262**, 856–859.
- 12 T. Ishiyama, J. Nishii, T. Yamashita, H. Kawazoe and T. Omata, *J. Mater. Chem. A*, 2014, **2**, 3940–3947.
- 13 T. Yamaguchi, T. Ishiyama, K. Sakuragi, J. Nishii, T. Yamashita, H. Kawazoe and T. Omata, *Solid State Ionics*, 2015, **275**, 22855–22861.
- 14 T. Yamaguchi, T. Ishiyama, K. Sakuragi, J. Nishii, T. Yamashita, H. Kawazoe, N. Kuwata, J. Kawamura and T. Omata, *Solid State Ionics*, 2016, **288**, 281–285.
- 15 T. Yamaguchi, T. Kataoka, S. Tsukuda, T. Ishiyama, J. Nishii, T. Yamashita, H. Kawazoe and T. Omata, *Phys. Chem. Chem. Phys.*, 2017, **19**, 29669–29675.
- 16 T. Yamaguchi, Y. Saito, Y. Kuwahara, H. Yamashita, T. Ishiyama, J. Nishii, T. Yamashita, H. Kawazoe and T. Omata, *J. Mater. Chem. A*, 2017, **5**, 12385–12392.
- 17 K. Kawaguchi, T. Yamaguchi, T. Omata, T. Yamashita, H. Kawazoe and J. Nishii, *Phys. Chem. Chem. Phys.*, 2015, **17**, 22855–22861.
- 18 T. Yamaguchi, S. Tsukuda, T. Ishiyama, J. Nishii, T. Yamashita, H. Kawazoe and T. Omata, *J. Mater. Chem. A*, 2018, **6**, 23628–23637.
- 19 T. Ishiyama, H. Kishimoto, K. Yamaji, T. Yamaguchi, J. Nishii, T. Yamashita, H. Kawazoe and T. Omata, *Int. J. Hydrogen Energy*, 2019, **44**, 24977–24984.
- 20 T. Nakamura, S. Mizunuma, Y. Kimura, Y. Mikami, K. Yamauchi, T. Kuroha, N. Taniguchi, Y. Tsuji, Y. Okuyama and K. Amezawa, *J. Mater. Chem. A*, 2018, **6**, 15771–15780.
- 21 I. Suzuki, M. Tashiro, T. Yamaguchi, T. Ishiyama, J. Nishii, T. Yamashita, H. Kawazoe and T. Omata, *Int. J. Hydrogen Energy*, 2020, **45**, 16690–16697.
- 22 T. Omata, T. Yamaguchi, S. Tsukuda, T. Ishiyama, J. Nishii, T. Yamashita and H. Kawazoe, *Phys. Chem. Chem. Phys.*, 2019, **21**, 10744–10749.
- 23 T. Kentaro, *J. Ceram. Assoc. Jpn.*, 1955, **63**, 142–147.
- 24 A. Makishima and J. D. Mackenzie, *J. Non-Cryst. Solids*, 1973, **12**, 35–45.
- 25 B. Deng, *J. Non-Cryst. Solids*, 2020, **529**, 119768.
- 26 S. Bishnoi, S. Singh, R. Ravinder, M. Bauchy, N. N. Gosvami, H. Kodamana and N. M. A. Krishnan, *J. Non-Cryst. Solids*, 2019, **524**, 119643.
- 27 N. Mascaraque, A. Durán and F. Muñoz, *J. Non-Cryst. Solids*, 2011, **357**, 3212–3220.
- 28 S. Le Roux, S. Martin, R. Christensen, Y. Ren and V. Petkov, *J. Phys.: Condens. Matter*, 2011, **23**, 035403.
- 29 R. K. Brow and D. R. Tallant, *J. Non-Cryst. Solids*, 1997, **222**, 396–406.
- 30 N. Boubata, A. Roula and I. Moussaoui, *Bull. Mater. Sci.*, 2013, **36**, 457–460.
- 31 I. V. Kozhevnikov and K. I. Matveev, *Appl. Catal.*, 1983, **5**, 135–150.
- 32 M. Makoto, *Mater. Chem. Phys.*, 2002, **75**, 103–120.
- 33 Y. Ansari, T. G. Tucker and C. A. Angell, *J. Power Sources*, 2013, **237**, 47–51.
- 34 Y. Ansari, T. G. Tucker, W. Huang, I. S. Klein, S. Y. Lee, J. L. Yarger and C. A. Angell, *J. Power Sources*, 2016, **303**, 142–149.

